Density-functional electronic structure calculations for native defects and Cu impurities in CdS

Kazume Nishidate,* Takuya Sato, Yuta Matsukura, Mamoru Baba, and Masayuki Hasegawa
Faculty of Engineering, Iwate University, Morioka 020-8551, Japan

Taizo Sasaki
National Institute for Materials Science, 1-2-1 Sengen, Tsukuba 305-0047, Japan
(Received 25 August 2005; revised manuscript received 17 April 2006; published 24 July 2006)

We performed density-functional electronic structure calculations for wurtzite CdS with native defects and Cu impurity. We investigate formation energies and ionization levels of the defects in various charge states. Our results reveal that the S vacancy is a double donor with the strongly localized orbital at the defect site, and could act as an intrinsic compensation defect under *p*-type doping. On the other hand, the interstitial S at the tetrahedral site is a double acceptor which forms into a dumbbell-like atomic configuration with the nearest S atom. The impurity Cu substituting Cd produces a single acceptor state, while the interstitial Cu generates a single donor state. The calculated formation energies imply that the donor state could also cause the compensation in the Cu doped CdS.

DOI: 10.1103/PhysRevB.74.035210 PACS number(s): 71.15.Mb, 71.20.Nr, 71.55.Gs, 71.70.Ej

I. INTRODUCTION

Cadmium sulfide (CdS), a member of II-VI wide-gap semiconducting compounds, is of considerable interest because of its potential applications to optoelectronic devices[1,2] and, for that reason, electronic structure calculations of the wurtzite CdS have been performed by several authors. First principles calculation using the norm-conserving pseudopotential with local-density approximation was performed by Chang, Froyen, and Cohen[3] in 1983 and the details of the valence band structure were investigated. More accurate calculations were performed by Vogel *et al.*[4] using relaxation-corrected pseudopotentials (SIRC-PPs) method with self-interaction correction and by Rohlfing *et al.*[5] using *GW* quasiparticle correction method. The energy of the deep Cd 4*d* state and the band gap was significantly improved by these calculations. Also, Lew Yan Voon *et al.*[6] investigated the effect of spin-orbit splitting using linear muffin-tin orbital method and found that its inclusion improves the energy width of the uppermost valence band.

Pristine CdS shows that the *n*-type conductivity and the formation of *p*-type CdS, which is important for the practical applications, is very difficult probably because of native defects. However, electronic and structural properties of the wurtzite CdS with native defects and impurity are not clear at present. It has been suggested that the *p*-type doping difficulty arises from the strong self-compensation effect due to sulfur vacancies[1,2,7] and the deep acceptor levels.[8] Until now, some authors reported that the Cu in-diffusion transforms *n*-type CdS to a highly compensated semi-insulating material[9–12] and finally to a *p*-type CdS with high Cu content.[13–15] Also, recent studies revealed that Cu doped CdS shows a favorable *p*-type characteristic.[16–19] In the present work we perform density-functional electronic structure calculations to investigate the formation energies and the ionization levels of native defects and Cu impurity and thereby provide a theoretical insight into the compensation mechanism of Cu doped CdS.

II. ELECTRONIC STRUCTURE OF CdS WITHOUT DEFECTS

The unit cell of wurtzite CdS is a hexagonal prism belonging to the space group $P6_3mc$ (No. 186) and contains four atoms as shown in Fig. 1. The Brillouin zone of wurtzite structure with high-symmetry points is shown in Fig. 2. Our calculations were performed using the first principles simulation code VASP.[20–23] The total energy was calculated using projector augmented-wave (PAW) method[24,25] together with the Perdew and Wang exchange-correlation functional (PW91) (Ref. 26) in the generalized gradient approximation. Spin-polarization effect is taken into account in the calculations of Cu related defects.

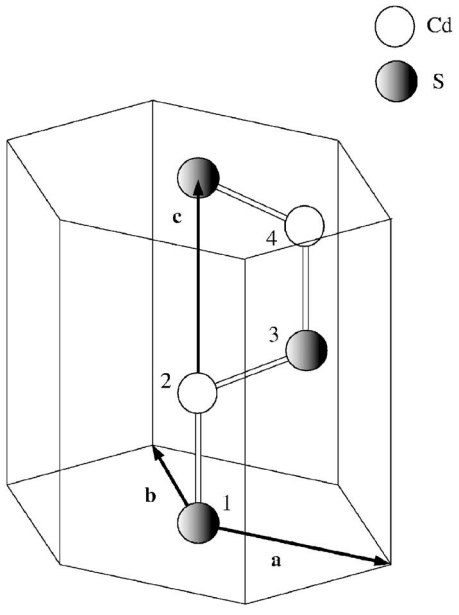

FIG. 1. Primitive unit cell of wurtzite CdS. Four atoms labeled 1–4 are at (0, 0, 0), $(0,0,u)$, $(\frac{1}{3},\frac{2}{3},0.5)$, and $(\frac{1}{3},\frac{2}{3},u+0.5)$, respectively. The lattice vectors are taken as $\mathbf{a}=(a,0,0)$, $\mathbf{b}=(-a/2,a\sqrt{3}/2,0)$, and $\mathbf{c}=(0,0,c)$. The values of the lattice parameters are given in Table I.

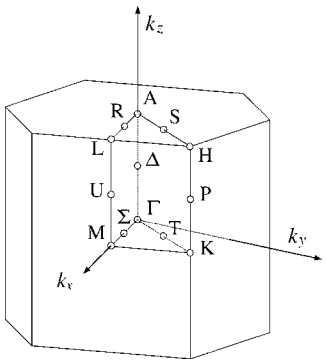

FIG. 2. Brillouin zone of wurtzite structure. Open circles show the high-symmetry points.

We first determined the equilibrium lattice parameters of the wurtzite CdS. The reciprocal space integration is carried out using 12^3 Monkhorst-Pack sampling[27] resulting in 133 reciprocal vectors in the irreducible part of Brillouin zone. Cutoff energy of 300 eV is used to obtain well converged total energy. The calculated optimal lattice parameters are in good agreement with experiments as shown in Table I, and these values are used throughout in our calculations for retaining self-consistency. Figure 3 shows electronic band structure and density of states of wurtzite CdS.

The calculated Kohn-Sham band gap energy E_g^{DFT} is 1.20 eV and about half of the experimentally observed optical band gap energy $E_g^{\mathrm{expt.}}$ of 2.42 eV at room temperature.[30] The underestimation of the gap energy $\Delta E_g \equiv E_g^{\mathrm{expt.}} - E_g^{\mathrm{DFT}}$ (=1.22 eV) is a well known shortcoming of density-functional electronic structure calculations for semiconducting materials. In Fig. 3, the lowest two energy bands around −12.1 eV with a narrow width of 0.6 eV and the next lowest ten bands around −7.2 eV with a rather large width of 1.1 eV originate from the S 3*s* state and Cd 4*d* state, respectively. It has been shown that the Cd 4*d* state shifts downward to −8.1 eV by the *GW* quasiparticle correction together with the Cd^{20+} pseudopotential[5] and to −9.6 eV by the SIRC-PPs,[4] which is well compared to the experimentally observed one around −9.5 eV.[31] The group of uppermost valence bands of 4.3 eV width arise from S 3*p* states and the lowest conduction band mainly from Cd 5*s* states. The calculated PAW band structure is in qualitative agreement with the experimental valence band obtained by Stoffel[31] using angle-resolved photoelectron spectroscopy except for the position of deep Cd 4*d* levels.

TABLE I. Optimized structural parameters of wurtzite CdS and their comparison with experimental results.

	a (Å)	c (Å)	c/a	u
Present work	4.199	6.826	1.626	0.377
Experimental	4.141[a]	6.720[a]	1.623	0.373[b]

[a]Reference 28.
[b]Reference 29.

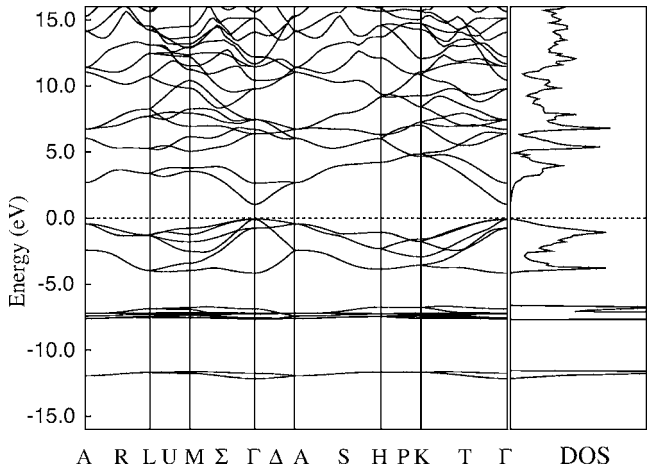

FIG. 3. Electronic band structure (left-hand side) and density of states (right-hand side) of wurtzite CdS obtained by the PAW method. Energy is measured relative to the valence band maximum (horizontal dashed line). The letters **A**–**Γ** denote high-symmetry points in the first Brillouin zone (Fig. 2).

III. NATIVE DEFECTS AND Cu IMPURITY

A. Computational details

Pristine CdS is known to show *n*-type characteristics due to the intrinsic defects.[1,2,7] To study the electronic structure of wurtzite CdS with defects, we performed a series of calculations using a supercell consisting of $3\times3\times2$ wurtzite CdS primitive unit cells, which contains 72 atoms in total. The use of a large hexagonal supercell considerably reduces the defect-defect interactions that arises from the interaction with periodic images. Good convergence was achieved using the cutoff energy of 300 eV. Only the Γ point was considered in the reciprocal space integrations during the structural optimization while the size and shape of the supercell were fixed. All the atoms were allowed to relax until the residual atomic force became less than 0.05 eV/Å. Total energies were evaluated using the 2^3 Monkhorst-Pack sampling in the reciprocal space of the supercell.

The formation energy of defects with charge q, $\Delta E^D(q)$, can be obtained from the total energy of the supercell containing the defect, $E^D(q)$, as

$$\Delta E^D(q) = E^D(q) - n_{\mathrm{Cd}}\mu_{\mathrm{Cd}} - n_{\mathrm{S}}\mu_{\mathrm{S}} - n_{\mathrm{Cu}}\mu_{\mathrm{Cu}} + q(\mu_{\mathrm{e}} + E_{\mathrm{VBM}}) + \xi(q). \quad (1)$$

Here, μ_{e} is the electron chemical potential that determines the Fermi level and varies in the range of the band gap; n_{A} and μ_{A} (A=Cd,S,Cu) are the number of atoms in the defective supercell and atomic chemical potential, respectively.

The energy of the valence band maximum, E_{VBM}, was adjusted so as to cancel the background charge neutralizing the defective supercell at the charge state q,[32–34]

$$E_{\mathrm{VBM}} = E_{\mathrm{VBM}}^{bulk} + \Delta V_{av}. \quad (2)$$

E_{VBM}^{bulk} is the energy cost in removing an electron from the perfect supercell and defined by

$$E_{\mathrm{VBM}}^{bulk} = E(0) - E(+1), \quad (3)$$

where $E(q)$ is the total energy of the perfect supercell at the charge state q $(=0,+1)$. ΔV_{av} is the averaged difference between the local potentials far from the defect in the defective supercell and the corresponding ones in the perfect supercell. We evaluated this term only at the charge neutral state and used it for all the charged states. The last term $\xi(q)$ in Eq. (1) is proportional to q^2 and accounts for the electrostatic energy of point charges in an oppositely charged homogeneous medium (jellium background).[35,36] We approximate $\xi(q)$ by a Madelung term divided by the dielectric constant of CdS (Ref. 37) to take account of the screening effect of the charge q in the host crystal environment.

The equilibrium constraint for the atomic chemical potentials is given by

$$\mu_{\mathrm{CdS}} = \mu_{\mathrm{Cd}} + \mu_{\mathrm{S}}, \quad (4)$$

where μ_{CdS} is the chemical potential of CdS and obtained as half of the total energy of the primitive unit cell. The *elemental* atomic chemical potentials, μ_{A}^0 [A=Cd,S, (molecule S_2), S (solid αS), Cu], are given as the total energies per atom of bulk Cd metal in the hcp structure, S_2 molecule at the spin triplet state, solid αS in the orthorombic structure,[38] and bulk Cu metal in the fcc structure, respectively. The total energies of these metals are calculated using 20^3 Monkhorst-Pack sampling mesh in the reciprocal space integration, while only the Γ point is used in the total energy calculation of the S_2 molecule in a 10^3 Å^3 cubic supercell. We use a rather sparse mesh, 2^3 sampling, in the reciprocal space integration of the solid αS due to its large size of the unit cell containing 128 atoms. Optimal (and the experimental) lattice constants, in Å unit, are a=10.418(10.465), b=12.848(12.866), and c =24.631(24.486), demonstrating a good consistency with the experiment.

The heat of formation (ΔH) of bulk CdS is the energy gain in forming the crystal and given by

$$\Delta H = \mu_{\mathrm{CdS}} - (\mu_{\mathrm{Cd}}^0 + \mu_{\mathrm{S}}^0), \quad (5)$$

which also specifies the range of the atomic chemical potentials with the constraint equation (4); the Cd-rich (S-rich) growth condition is achieved by putting $\mu_{\mathrm{Cd}} \rightarrow \mu_{\mathrm{Cd}}^0$ and $\mu_{\mathrm{S}} \rightarrow \mu_{\mathrm{S}}^0 + \Delta H$ ($\mu_{\mathrm{S}} \rightarrow \mu_{\mathrm{S}}^0$ and $\mu_{\mathrm{Cd}} \rightarrow \mu_{\mathrm{Cd}}^0 + \Delta H$), respectively. Note that the atomic chemical potential of sulfur in the S-rich condition also depends on its elemental form, molecule or solid, used in the evaluation of the μ_{S}. When we adopt the atomic chemical potential of sulfur obtained by the S_2 molecule in the vacuum ΔH becomes 1.90 eV, while it lowers to 1.35 eV in the case of the solid αS. These results of heat of formation are compared to the experimental one [1.68 eV (Ref. 30)] and we use these two values in the S-rich case.

TABLE II. Number of electrons m following the CBM at the respective charge state q.

q	Cd_S	V_S	Cd_i^{oct}	Cu_i^{oct}
−2	4	2	4	3
−1	3	1	3	2
0	2		2	1
+1	1		1	

The atomic chemical potential of copper, μ_{Cu}, is fixed at the value evaluated in its metallic state, μ_{Cd}^0, which implies that the system is exposed to the Cu-rich environment. This situation may correspond to the actual formation process, where CdS was deposited and grown on the metallic Cu thin film and then annealed to cause Cu diffusion into CdS.[16–19]

Among the possible defects in the wurtzite structure,[39] six types of isolated native defects are considered, namely, (i) Cd vacancy (V_{Cd}), (ii) S vacancy (V_{S}), (iii) Cd interstitial (Cd_i), (iv) S interstitial (S_i), (v) Cd antisite (Cd_S), and (vi) S antisite (S_{Cd}). We also considered Cu interstitial (Cu_i) and substitutional Cu at the Cd site (Cu_{Cd}) associated with the copper impurity. Here, V_{Cd} (V_{S}) is generated by removing one Cd (S) atom from the supercell, and Cd_i (S_i) is generated by inserting one Cd (S) atom into an interlattice space of the supercell. In the wurtzite structure of the CdS, octahedral and tetrahedral sites are known as possible interstitial sites. The octahedral site is located at $\left(\frac{2}{3},\frac{1}{3},u/2\right)$ in the unit cell coordinate system, which is the center of mass of the closely interpenetrating two octahedra, each containing six Cd and six S atoms, respectively. The distance from the octahedral site to the nearest neighbor atoms is 2.74 Å, and that to the next nearest neighbor atoms is 3.22 Å. On the other hand, the tetrahedral site is located at $\left(\frac{1}{3},\frac{2}{3},u/2\right)$ in the unit cell coordinates system and it is the center of mass of the closely interpenetrating two tetrahedra, each containing four Cd and four S atoms, respectively. The distances from the tetrahedral site to the nearest and the next nearest neighbor atoms are 2.13 and 2.74 Å, respectively.

One Cu atom is placed at an interstitial site for the Cu_i, and one Cd atom is replaced by one Cu for the Cu_{Cd}. These configurations correspond to Morigaki's isolated Cu-A and Cu-B centers, respectively, and have been experimentally investigated by electron paramagnetic resonance.[40,41] Davies *et al.*[42] proposed a center consisting of substitutional Cu and an unknown impurity or defect, but we do not consider such a defect complex in this work.

Our calculations revealed that the octahedral site is slightly more favorable for the Cd and Cu interstitials while the S interstitial favors the tetrahedral site, all in their charge neutral states. Therefore, we present only the results for the stable interstitials, namely, Cd_i^{oct}, Cu_i^{oct}, and S_i^{tet}. We adopt the experimental band gap $E_g^{\mathrm{expt.}}$ rather than the theoretical one E_g^{DFT}. This implies that the energy levels of the acceptor defects which follow the valence band maximum (VBM) are unchanged while those of the donor defects following the

conduction band minimum (CBM) are corrected,[43] i.e., the formation energies of the donor defects, Cd_S, V_S, Cd_i^{oct}, and Cu_i^{oct} are corrected by adding $m \times \Delta E_g$, where m is the number of electrons following the CBM as inspected by the charge density maps. We summarize the values of m for the defect-induced levels in Table II. Here the V_S at the neutral state is not corrected ($m=0$) since it has a strongly localized VBM-like character as shown later (Fig. 6).

Thermal ionization energy $\epsilon(q/q')$ is the Fermi-level position μ_e at which the charge state changes from q to q' as μ_e rises in the gap, where each of the atomic configurations are fully relaxed. Note that the optical level observed in photoluminescence would be different from the thermal ionization level since the atomic configuration is maintained during the Frank-Condon type transition process.[44] Even in this case, the subsequent thermal relaxation process will bring the atomic system to an equilibrium configuration.

B. Defect formation energies

Figure 4 shows the calculated defect formation energies at (a) S (molecule S_2)-rich, (b) S (solid αS)-rich, and (c) Cd-rich conditions, respectively. The node of each solid line in these figures corresponds to the thermal ionization level $\epsilon(q/q')$ and is schematically shown in Fig. 5. We can see that μ_S (solid αS) is less favorable than μ_S (molecule S_2) to achieve the limit of S-rich condition. When μ_e is at the VBM ($\mu_e=0$ eV), the system is in the p-type electronic environment and the stable charge states of the defects both in the S-rich and Cd-rich conditions are found to be $(Cd_S)^{+2}$, $(V_S)^{+2}$, $(Cd_i^{oct})^{+2}$, $(V_{Cd})^0$, $(S_i^{tet})^0$, and $(S_{Cd})^0$. On the other hand, when μ_e is at the CBM ($\mu_e=2.42$ eV) and hence the system is in the n-type electronic environment, the stable charge states become $(Cd_S)^0$, $(V_S)^0$, $(Cd_i^{oct})^0$, $(V_{Cd})^{-2}$, $(S_i^{tet})^{-2}$, and $(S_{Cd})^{-2}$. Among the donor-type defects (Cd_S, V_S, and Cd_i^{oct}), the formation energy of V_S is relatively low both in the S-rich and Cd-rich conditions. This indicates that the native defect V_S could be a dominant donor center and acts as an intrinsic compensation source under the p-type doping. Figure 6 shows the three-dimensional electron orbital map of the highest occupied energy level of the defect V_S at the charge neutral state. We can clearly see the strongly localized orbital at the vacancy site and the VBM-like p orbitals at the nearest neighbor S sites in the direction to the vacancy. The formation of the localized orbitals at the defect state is very similar to that of the oxygen vacancy in ZnO.[45,46] The antisite Cd_S produces the charge neutral state below the CBM and could also become an effective electron source, but its formation energy is very high at the S-rich condition. The interstitial Cd_i^{oct} produces two ionization levels, $\epsilon(+2/+1)$ and $\epsilon(+1/0)$. On the other hand, the vacancy V_{Cd} produces a neutral state above the VBM. The formation energy of V_{Cd} is the lowest in the n-type environment. The defects S_i^{tet} and S_{Cd} also produce acceptor states but their formation energies are higher than that of V_{Cd} in the range of $\mu_e \geq 0.5$ eV.

Distances from the defect site to the surrounding ions at the respective charge state are summarized in Table III. Antisite defect Cd_S is surrounded by four Cd atoms. The tetrahedron made of the ligands of the defect is enlarged isotro-

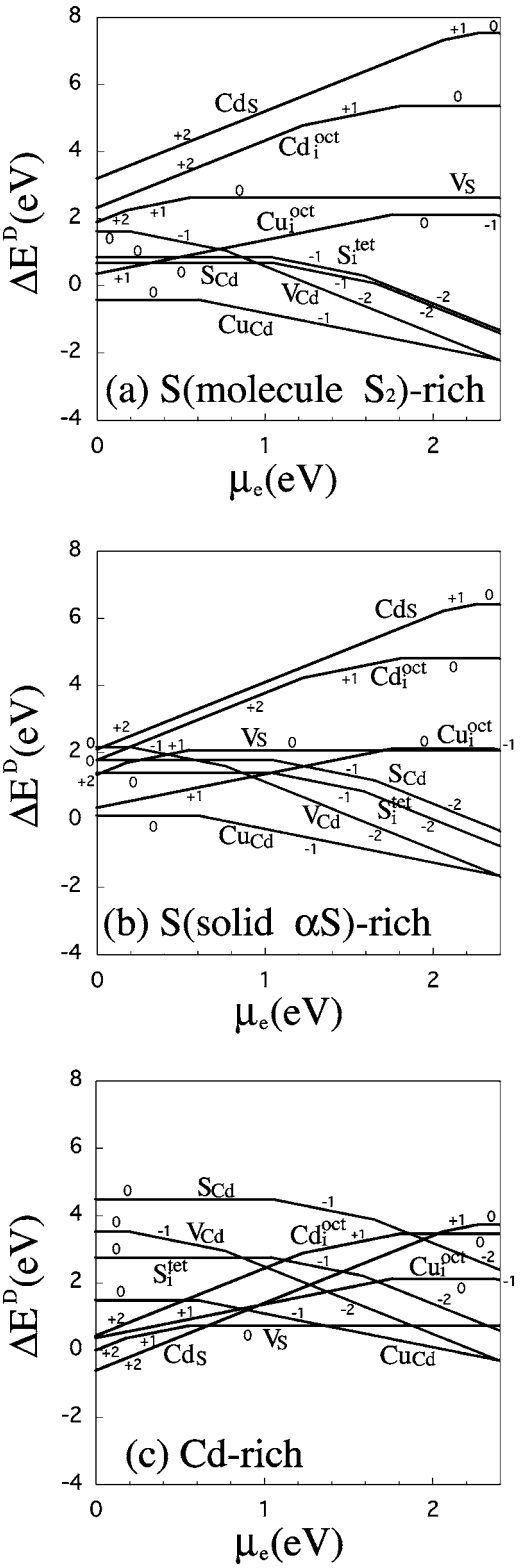

FIG. 4. Defect formation energies in the (a) S(molecule S_2)-rich, (b) S(solid αS)-rich, and (c) Cd-rich conditions, respectively. The μ_e is the electronic chemical potential which varies in the band gap, from the VBM to the CBM. The number on each curve shows the stable charge state.

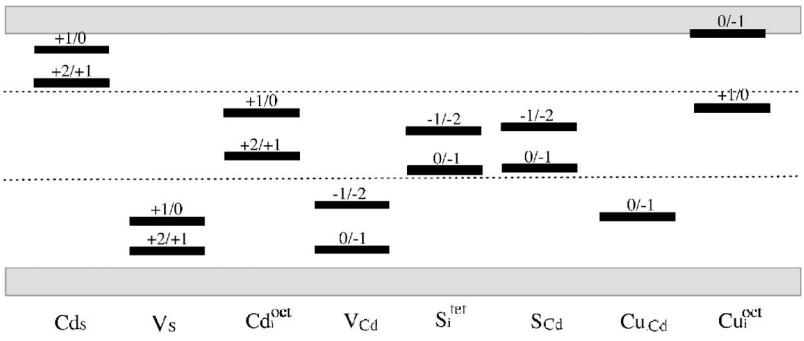

FIG. 5. Thermal ionization levels $\epsilon(q/q')$ in the energy band gap between the VBM (lower thick line) and the CBM (upper thick line), where (q/q') denotes the position at which charge state changes from q to q' as the chemical potential μ_e increases (Fig. 4). The energies of 1 and 2 eV measured from the VBM are indicated by the dotted lines.

pically as the charge q changes from +2 to 0. The nearest neighbor atoms of the Cd_i^{oct} depart from the defect site as the charge state changes from +2 to 0, while the other neighboring atoms approach the defect site. This can be understood by the localized nature of electrons at the defect site and the electrostatic interactions with the neighboring ions. The vacancy V_S shows a quite different feature and attracts the nearest neighbors more strongly as the charge state changes from +2 to 0. This indicates that the strongly localized orbital at the vacacy site (Fig. 6) attracts the neighboring positive Cd ions by the electrostatic force and induces the inward lattice deformation. Antisite defect S_{Cd}, however, has only three nearest neighbors, in contrast to the case of Cd_S; the fourth sulfur ligand of the site departs from the neighboring space. The distances between the defect site and the neighboring ions are almost unchanged when the charge state changes from $q=0$ to -2.

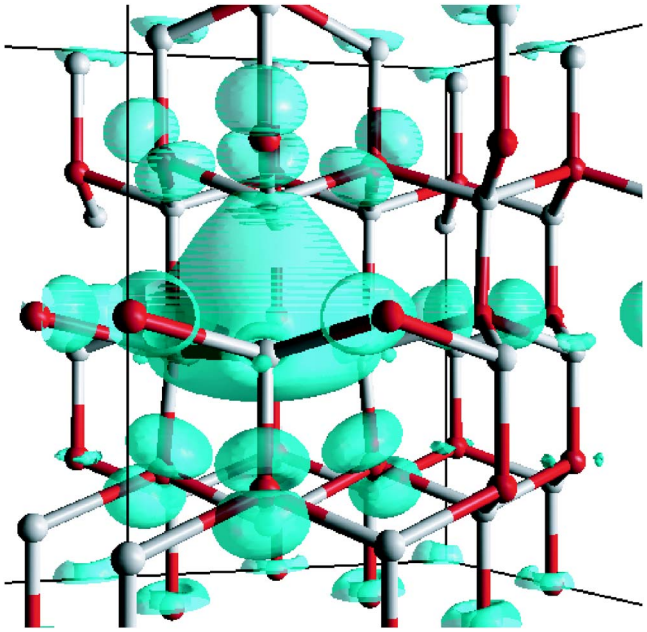

FIG. 6. (Color online) Localized electron orbital of the highest occupied state of the defect V_S at the charge neutral state. Only the surfaces with the concentration 15% of the maximum charge density are shown. The framework made of the rods and spheres represents the geometry of the defective supercell. The red (dark gray) and white (light gray) spheres indicate the sulfur and cadmium sites, respectively. The solid lines are the outlines of the supercell. There is a strongly localized orbital at the V_S site (central part), while VBM-like p orbitals are formed at the neighboring S sites in the direction to the vacancy. For clarity, only these sections are shown for these orbitals on this side.

After the structural relaxation, the interstitial S_i^{tet} forms a dumbbell-like atomic configuration with the nearest S atom (Fig. 7) and the distances between them 2.06 Å is unchanged for the change in charge state from 0 to −2. The interstitial has three bonds: one with the nearest S forming the dumbbell geometry and two with the Cd atoms. These bonds are almost on the same plane, implying the formation of sp^2-hybrid orbitals. Similar atomic configuration has been reported for the oxygen interstitial in ZnO,[47] where the strong O-O bond was attributed to the formation of a $sp^2\sigma$ orbital. The present result indicates that the physical origin of the defect S_i^{tet} in CdS is the same as that of the oxygen interstitial with dumbbell-like atomic configuration in ZnO.

C. Copper impurities

Substitutional Cu on a Cd site is expected to be a single acceptor (group-IB element substitutes group-IIB element). The ionization level $\epsilon(0/-1)$ is located 0.6 eV above the VBM (Figs. 4 and 5). When μ_e is at the VBM, the stable charge states are found to be $(Cu_{Cd})^0$ and $(Cu_i^{oct})^{+1}$. On the other hand, when μ_e is at the CBM, the stable states become $(Cu_{Cd})^{-1}$ and $(Cu_i^{oct})^{-1}$. The small formation energy of this defect in the S-rich condition implies that Cu_{Cd} is a potential candidate for an effective hole source of the p-type conductivity. Here the electronic configuration of Cu_{Cd} at the $q=0$ state is $3d^9 4(s-p)^2$. Its net ionicity in the host crystal is Cu^{+2} in its core region. Correspondingly, Cu_{Cd} at the $q=-1$ state has the electronic configuration $3d^{10}4(s-p)^2$ with the net ionicity of Cu^+ in its core region. The $3d$ orbitals are well localized around the copper. On the other hand, interstitial Cu is expected to be a single donor. In our calculation, the interstitial Cu_i^{oct} has two ionization levels; one is the $\epsilon(+1/0)$ at 0.7 eV below the CBM, and the other is the $\epsilon(0/-1)$ just below the CBM. However, that acceptor state is very close to the CBM and seems to be an artificial one due to the effect of the band gap correction Nevertheless, the results indicate that the Cu on the interstitial site behaves as a single donor and becomes a single acceptor in the cation substitution.

It has been experimentally known that the Cu in-diffusion transforms n-type CdS into a highly compensated material.[9–12] Since the suggestion of Mandel *et al.*[48] in 1964, it has been believed that the *self-compensation* by native

TABLE III. Distances between the defect site and the surrounding ions (numbers in the parentheses in units of Å). The initial distances before the structural relaxations are given in the row *initial*. The numbers +2– −2 show the charge states q. The integers in front of the letters S, Cd, and Cu are the numbers of surrounding ions within the distance of 3.2 Å from the defect. The initial site of the vacancy is assumed to be on the ideal site of the removed atom.

	Initial	+2	+1	0
Cd_S	4Cd(2.57)	3Cd(3.02)	3Cd(3.05)	3Cd(3.07)
		Cd(3.12)	Cd(3.10)	Cd(3.08)
Cd_i^{oct}	3Cd(2.74), 3S(2.74)	3S(2.63)	3S(2.66)	3S(2.71)
		3Cd(3.02)	3Cd(2.99)	3Cd(2.96)
V_S	4Cd(2.57)	3Cd(3.16)	Cd(3.13)	3Cd(2.25)
		Cd(3.17)	3Cd(3.14)	Cd(2.36)
	Initial	0	−1	−2
S_i^{tet}	Cd(2.13), S(2.13)	S(2.06)	S(2.06)	S(2.06)
	3Cd(2.74), 3S(2.74)	2Cd(2.53)	2Cd(2.54)	2Cd(2.55), Cd(3.12)
S_{Cd}	4S(2.57)	3S(2.35)	3S(2.36)	3S(2.37)
V_{Cd}	4S(2.57)	S(2.42)	4S(2.48)	S(2.41)
		3S(2.49)		3S(2.42)
	Initial	+1	0	−1
Cu_i^{oct}	3S(2.74), 3Cd(2.74)	3S(2.34)	3S(2.35)	3S(2.35)
		3Cd(2.80)	3Cd(2.79)	3Cd(2.77)
Cu_{Cd}	4S(2.57)		1S(2.36)	1S(2.37)
			3S(2.37)	3S(2.38)

defects is the origin of the doping difficulties in large band gap semiconductors. In the case of CdS, V_S is the most plausible candidate for the source of the self-compensation. However, the analysis by Neumark[39,49] showed that similar compensation behavior in large band gap semiconductors could result from amphoteric impurities. Our calculations actually indicate that the *p*-type doping difficulties with Cu in CdS could also result from the compensation by the donor state of the interstitial Cu.

In CdS, Cd occupies the tetrahedral coordination with the C_{3V} point symmetry. The tetrahedron is composed of four S ions and slightly distorted along the *c* axis. When Cu is incorporated onto the Cd site (Cu_{Cd}), the lattice distortion due to the crystal field is expected to occur. On the other hand, the Cu interstitial site is surrounded by the two interpenetrating octahedrons, one made of Cd ions and the other of S ions. In such a situation, electrostatic interactions between the copper and the ligands (Cd and S) may play an important role in stabilizing the local geometry. The distances from the Cu to the surrounding ions at the respective charge states for Cu_i^{oct} and Cu_{Cd} are also presented in Table IV. We can see that the Cu_i^{oct} strongly attracts S ions while repels Cd ions, leading to the shrinkage of the octahedron. When the charge state of Cu_i^{oct} changes from +1 to −1, its distance to the S ions (Cd ions) increases (decreases) because of the electrostatic interactions induced by the localized charge of the copper. In the case of the Cu_{Cd}, we also observe a significant shrinkage of the distorted tetrahedron surrounding the copper. In both cases, Cu attracts S ligands and repels Cd ligands.

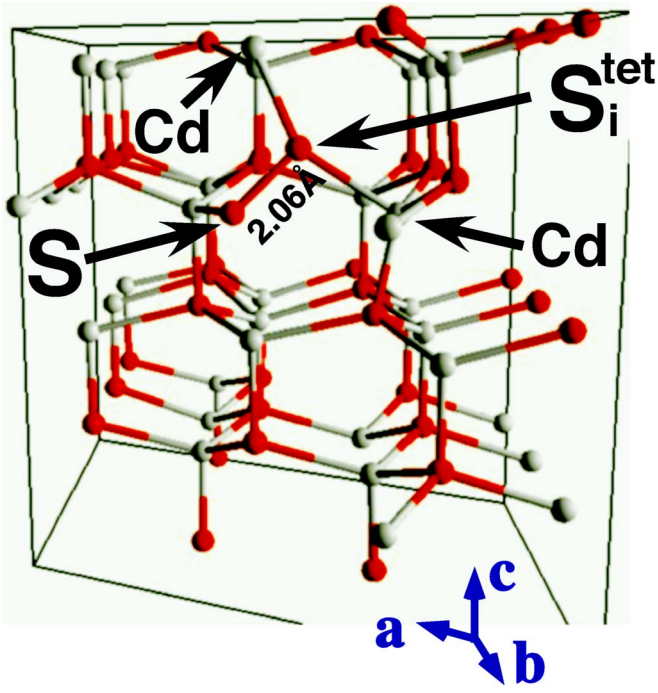

FIG. 7. (Color online) Interstitial S_i^{tet} forming a dumbbell-like atomic configuration with the nearest S atom. The framework made of the rods and spheres represents the geometry of the defective supercell. The red (dark gray) and white (light gray) spheres indicate the sulfur and cadmium sites, respectively. The solid lines are the outlines of the supercell.

TABLE IV. Distances from the copper atom to the surrounding ions (numbers in the parentheses in unit of Å) in Cu_i^{oct} and Cu_{Cd}. The initial distances before the structural relaxations are given in the row *initial*. The numbers +1, 0, and −1 show the charge states. The integers in front of the letters S and Cd are the numbers of surrounding ions within the distance of 3.2 Å from the copper.

	Initial	+1	0	−1
Cu_i^{oct}	3S(2.74)	3S(2.34)	3S(2.35)	3S(2.35)
	3Cd(2.74)	3Cd(2.80)	3Cd(2.79)	3Cd(2.77)
Cu_{Cd}	4S(2.57)		1S(2.36)	1S(2.37)
			3S(2.37)	3S(2.38)

IV. CONCLUSIONS

We have performed electronic structure calculations of wurtzite CdS with native defects and Cu impurity to investigate the underlying mechanism of the *p*-type doping difficulty in the Cu doped CdS. In these investigations, we considered six types of isolated native defects, i.e., V_{Cd}, V_S, Cd_i, S_i, Cd_S, and S_{Cd}. The defects Cu_i and Cu_{Cd} associated with the copper impurity were also studied. It was found that the cation interstitials Cd_i and Cu_i favor the octahedral site while the anion interstitial S_i favors the tetrahedral site where it forms into a dumbbell-like atomic configuration with the nearest S atom. Among the donor type defects, V_S shows the lowest formation energy and therefore could act as an intrinsic compensation defect under *p*-type doping. The substitutional Cu generates an acceptor level and its formation energy is very low at the S-rich condition, implying that Cu_{Cd} becomes an effective hole source for the *p*-type conductivity. We also found that the Cu_i^{oct} generates donor states. These results indicate that the Cu impurity in the interstitial site behave as a donor but becomes an acceptor in the cation substitution. This donor state could also cause the compensation in the Cu doping in CdS.

ACKNOWLEDGMENTS

The authors acknowledge Y. Kashiwaba for a valuable discussion. We are also grateful to H. Toriyabe, D. Yokota, R. Yokoyama, and K. Ohta for assistance in the computations. This work was supported by a Grant-in-Aid for Scientific Research from the Ministry of Education, Culture, Sports, Science and Technology through Grant Nos. 16550002 and 16540301. The computations in the present work were performed using the facilities of the Supercomputer Center, Institute for Solid State Physics, University of Tokyo, and the Information Processing Center of Iwate University.

*Electronic address: nisidate@iwate-u.ac.jp

[1] A. L. Fahrenbruch and R. H. Bube, *Fundamentals of Solar Cells* (Academic Press, New York, 1983).
[2] K. L. Chopra and S. R. Das, *Thin Film Solar Cells* (Plenum Press, New York, 1983).
[3] K. J. Chang, S. Froyen, and M. L. Cohen, Phys. Rev. B **28**, 4736 (1983).
[4] D. Vogel, P. Krüger, and J. Pollmann, Phys. Rev. B **54**, 5495 (1996).
[5] M. Rohlfing, P. Krüger, and J. Pollmann, Phys. Rev. Lett. **75**, 3489 (1995).
[6] L. C. LewYan Voon, M. Willatzen, M. Cardona, and N. E. Christensen, Phys. Rev. B **53**, 10703 (1996).
[7] G. Mandel, Phys. Rev. **134**, A1073 (1964).
[8] R. H. Bube, *Photoconductivity of Solids* (Wiley, New York, 1960).
[9] G. A. Sullivan, Phys. Rev. **184**, 796 (1969).
[10] U. V. Desnica, I. D. Desnica-Franković, R. Magerle, A. Burchard, and M. Deicher, in *Materials Science Forum* (Trans Tech Publications, Switzerland, 1997), Vols. 258-263, p. 1347.
[11] I. D. Desnica-Franković, U. V. Desnica, A. Stötzler, and M. Deicher, Physica B **273-274**, 887 (1999).
[12] U. V. Desnica, I. D. Desnica-Franković, R. Magerle, and M. Deicher, Physica B **273-274**, 907 (1999).
[13] H. G. Grimmeis and R. Memming, J. Appl. Phys. **33**, 2217 (1962).
[14] W. Anderson and J. Mitchel, Appl. Phys. Lett. **12**, 334 (1968).
[15] M. Lichtensteiger, I. Lagnado, and H. C. Gatos, Appl. Phys. Lett. **15**, 418 (1969).
[16] Y. Kashiwaba, I. Kanno, and T. Ikeda, Jpn. J. Appl. Phys., Part 1 **31**, 1170 (1992).
[17] Y. Kashiwaba, H. Kirita, H. Abe, and T. Ikeda, Jpn. J. Appl. Phys., Part 1 **29**, 1733 (1990).
[18] Y. Kashiwaba, A. Tada, and T. Ikeda, Jpn. J. Appl. Phys., Part 2 **33**, L1613 (1994).
[19] T. Abe, Y. Kashiwaba, M. Baba, J. Imai, and H. Sasaki, Appl. Surf. Sci. **175-176**, 549 (2001).
[20] G. Kresse and J. Hafner, Phys. Rev. B **47**, R558 (1993).
[21] G. Kresse and J. Hafner, Phys. Rev. B **49**, 14251 (1994).
[22] G. Kresse and J. Furthmüller, Comput. Mater. Sci. **6**, 15 (1996).
[23] G. Kresse and J. Furthmüller, Phys. Rev. B **54**, 11169 (1996).
[24] G. Kresse and D. Joubert, Phys. Rev. B **59**, 1758 (1999).
[25] P. E. Blöchl, Phys. Rev. B **50**, 17953 (1994).
[26] J. P. Perdew and Y. Wang, Phys. Rev. B **45**, 13244 (1992).
[27] H. J. Monkhorst and J. D. Pack, Phys. Rev. B **13**, 5188 (1976).
[28] N. A. Razik, J. Mater. Sci. Lett. **6**, 1443 (1987).
[29] J. Camacho and A. Cantarero, Phys. Status Solidi B **215**, 181 (1999).
[30] *CRC Handbook of Chemistry and Physics*, 82nd ed. (CRC Press, New York, 2001).
[31] N. G. Stoffel, Phys. Rev. B **28**, 3306 (1983).
[32] D. B. Laks, C. G. Van de Walle, G. F. Neumark, P. E. Blöchl, and S. T. Pantelides, Phys. Rev. B **45**, 10965 (1992).
[33] S. Pöykkö, M. J. Puska, and R. M. Nieminen, Phys. Rev. B **53**, 3813 (1996).
[34] K. Matsunaga, T. Tanaka, T. Yamamoto, and Y. Ikuhara, Phys. Rev. B **68**, 085110 (2003).
[35] G. Makov and M. C. Payne, Phys. Rev. B **51**, 4014 (1995).

[36] M. Wardle, J. Goss, and P. R. Briddon, Phys. Rev. B **72**, 155108 (2005).
[37] O. Madelung, *Semiconductors: Data Handbook*, 3rd ed. (Springer, New York, 2004), p. 225.
[38] S. Retting and J. Trotter, Acta Crystallogr., Sect. C: Cryst. Struct. Commun. **C43**, 2260 (1987).
[39] G. F. Neumark, Mater. Sci. Eng., R. **R21**, 1 (1997).
[40] K. Morigaki, in *II-VI Semiconducting Compounds*, Proceedings of the 1967 International Conference, edited by D. G. Thomas (Benjamin, New York, 1967), p. 1348.
[41] K. Morigaki, J. Phys. Soc. Jpn. **19**, 1240 (1964).
[42] J. J. Davies, R. T. Cox, and J. E. Nicholls, Phys. Rev. B **30**, 4516 (1984).
[43] S. B. Zhang, S. H. Wei, A. Zunger, and H. Katayama-Yoshida, Phys. Rev. B **57**, 9642 (1998).
[44] S. Lany and A. Zunger, Phys. Rev. B **72**, 035215 (2005).
[45] A. F. Kohan, G. Ceder, D. Morgan, and Chris G. Van de Walle, Phys. Rev. B **61**, 15019 (2000).
[46] E. C. Lee, Y. S. Kim, Y. G. Jin, and K. J. Chang, Phys. Rev. B **64**, 085120 (2001).
[47] P. Erhart, A. Klein, and K. Albe, Phys. Rev. B **72**, 085213 (2005).
[48] G. Mandel, Phys. Rev. **134**, A1073 (1964).
[49] G. F. Neumark, J. Appl. Phys. **51**, 3383 (1980).